Results in Control and Optimization 12 (2023) 100246

Contents lists available at ScienceDirect

Results in Control and Optimization

journal homepage: www.elsevier.com/locate/rico

COVID-19 SIR model: Bifurcation analysis and optimal control

Mostak Ahmed [a,b,*], Md. Harun-Or-Rashid Khan [a], Md. Manirul Alam Sarker [b]

[a] Department of Mathematics, Jagannath University, Dhaka, 1100, Bangladesh
[b] Department of Mathematics, Bangladesh University of Engineering and Technology, Dhaka, 1000, Bangladesh

ARTICLE INFO

Keywords:
COVID-19
Direct–indirect transmission
Bifurcation
Asymptotic stability
Pontryagin's maximum principle
Optimal control

ABSTRACT

This paper proposes a SIR epidemic model with vital dynamics to control or eliminate the spread of the COVID-19 epidemic considering the constant population, saturated treatment, and direct–indirect transmission rate of the model. We demonstrate positivity, boundness and calculate the disease-free equilibrium point and basic reproduction number from the model. We use the Jacobian matrix and the Lyapunov function to analyze the local and global stability, respectively. It is observed that indirect infection increases the basic reproduction number and gives rise to multiple endemic diseases. We perform transcritical, forward, backward, and Hopf bifurcation analyses. We propose two control parameters (Use of face mask, hand sanitizer, social distancing, and vaccination) to minimize the spread of the coronavirus. We use Pontryagin's maximum principle to solve the optimal control problem and demonstrate the results numerically.

1. Introduction

An unknown cause first emerged in late December 2019 in Wuhan, Hubei Province, China. The WHO named the disease COVID-19 and caused the virus identified by Severe Acute Respiratory Syndrome Coronavirus 2 (SARS-CoV-2) [1]. Governments have taken various measures to protect their cities or countries, however, global migration has spread the disease around the world. The COVID-19 disease affects the lower respiratory tract, manifesting as the common cold and flu, causing severe pneumonia in humans, with fever being the most common side effect. COVID-19 spreads quickly from an infected person through personal contact, sneezing, or speaking.

The global outbreak has resulted in overall morbidity, with a mortality rate of approximately 4% and cases increasing rapidly in the US countries affected by the outbreak. It is followed by Spain, Italy and France [2], where millions of people were forced into isolation and harsh conditions by national governments. The disease was rapidly increasing in many countries worldwide. Vaccinations, self-isolation, medical treatment and wearing masks have been the most effective strategies for mitigating and fighting the outbreak of COVID-19.

Therefore, mathematical models are needed to separately estimate direct and indirect disease transmission, survival, mortality and other important variables for different countries. Many countries in the world try to take effective steps to control the spread of the COVID-19 epidemic. Especially in densely populated countries such as Bangladesh and India, it is difficult to control or reduce the spread of COVID-19 due to insufficient specific symptoms, unavailability of epidemiological patterns and genome sequences, inadequate injection vaccination and lack of awareness of treatment. Recently, many studies have adopted a simulation approach, using real data from relevant countries and depending on their current situation, the results of intervention laws differ in different countries and investigate different models as a function of transmission in different countries [3].

* Corresponding author at: Department of Mathematics, Jagannath University, Dhaka, 1100, Bangladesh.
E-mail address: mostak@math.jnu.ac.bd (M. Ahmed).

https://doi.org/10.1016/j.rico.2023.100246
Received 28 November 2022; Received in revised form 9 April 2023; Accepted 28 May 2023
Available online 1 June 2023

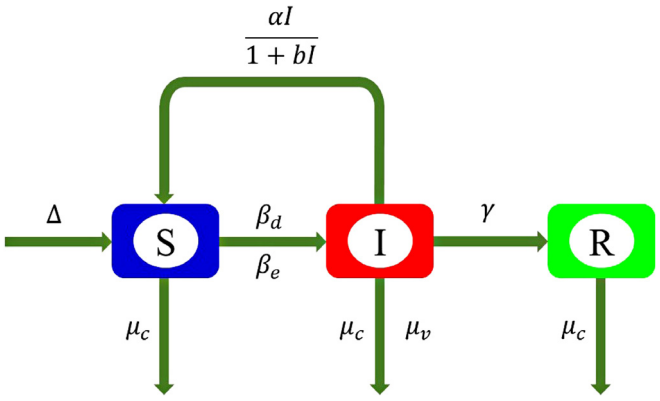

Fig. 1. Flowchart of the proposed COVID-19 SIR Model.

Constructed mathematical models to understand and predict epidemics, program Management Strategies and Policies [4,5]. Epidemiological models help us understand and hypothesize to predict when or how a disease will break out or die and provide important information on what to do to reduce the COVID-19 virus [6–9]. The epidemiological SIR model [10] has three compartments susceptible, infected and recovered. Many authors used different form models to control or reduce the spread of diseases in the community [11–14]. To avoid the shortage of treatment facilities they use treatment functions in their model [15]. Recently, many researchers analyzed their COVID-19 model with backward [16], forward–backward [17,18], transcritical [19], Hopf [20] bifurcations. With their model, they used optimal control variables to reduce COVID-19 [21,22] such as treatment, infection prevention, and vaccination.

Here, we build a SIR model with vital dynamics [23], including infection caused by direct or indirect contact between susceptible and infected individuals. We use a treatment function with a delayed constant parameter in the model [24]. We show that our system has transcritical, forward, backward and Hopf bifurcations by using theoretical and mathematical analysis. We enhanced our model with two control face masks, hand sanitizer, social distancing, and vaccinations to reduce transmission. We set up an optimal control function on our improved control model and using Pontryragin's maximum principle. Find the best strategies to control or reduce COVID-19 and demonstrate some results to show the effectiveness of our proposed control.

To the best of the authors' knowledge, this article presents for the first time all forward, backward, transcritical and Hopf bifurcations in the proposed COVID-19 SIR model. For the first time, we use a direct-indirect transmission model with two controls (face mask, hand sanitizer, social distancing, and vaccination use) to further reduce COVID-19.

2. Mathematical framework

The proposed COVID-19 SIR model system establishes a relationship between compartment model equations for susceptibility, infection and recovery. Model population $N(t)$ is subdivided as susceptible individuals $S(t)$, infected individuals $I(t)$ and recovered individuals $R(t)$ as shown in Fig. 1, where $N(t) = S(t) + I(t) + R(t)$. Considering the recruitment rate Δ (by birth) is constant and enters the susceptible population. The infection parameter is defined as the product of the average number of meetings between susceptible and infected individuals per time interval δt, denoted as m_i. The probability of successful infection is denoted by s_c. Thus, infection by direct contact between S and I individuals is given by $\frac{m_i s_c}{S+I} SI$ [25]. Simply write $m_i s_i = \beta_d$. In contrast to the previous direct transmission, indirect transmission is considered in this paper to be transmitted through the sneezes, and coughs of an infected person without contact. $\beta_e SI$ is considered indirect transmission from susceptible and infected individuals, where $\beta_e > 0$ is the indirect transmission rate. Likewise, numerous experimenters say that treatment is a vital measure in controlling the disease. Unfortunately, medical resources to control COVID-19 are limited in terms of staff numbers, hospital beds, test kits, oxygen cylinders and many other factors. To accommodate this, we use the treatment function $T(I) = \frac{\alpha I}{1+bI}$, where $b > 0$ is the saturation parameter and α is the cure rate [15]. For all assumptions and parameter definitions, we construct the following differential equation model:

$$\begin{aligned}
\frac{dS}{dt} &= \Delta - \frac{\beta_d SI}{S+I} - \beta_e SI - \mu_c S + \frac{\alpha I}{1+bI}, & S(0) &= S^0,\\
\frac{dI}{dt} &= \frac{\beta_d SI}{S+I} + \beta_e SI - \frac{\alpha I}{1+bI} - (\mu_c + \mu_v + \gamma) I, & I(0) &= I^0,\\
\frac{dR}{dt} &= \gamma I - \mu_c R, & R(0) &= R^0,
\end{aligned} \tag{1}$$

where γ, μ_c and μ_v are the rate of natural recovery, natural death and death due to coronavirus respectively.

2.1. Analysis of the proposed model

In this subsection, we have analyzed the proposed COVID-19 SIR model positivity property, boundedness property, basic reproduction number, disease-free equilibrium and stability analysis.

2.1.1. Model positivity property

Theorem 1. *The system (1) solutions are non-negative for $t > 0$ at $(S^0, I^0, R^0) \geq 0$.*

Proof. Since $N - R = S + I$. The first equation of the system (1) can be written as:

$$\frac{dS(t)}{dt} = \Delta - \frac{\beta_d S(t)\epsilon(t)}{\rho(t)} - \beta_e S(t)\epsilon(t) - \mu_c S(t) + \frac{\alpha\epsilon(t)}{1 + b\epsilon(t)}, \tag{2}$$

where $\rho(t) = N(t) - R(t)$ and $\epsilon(t) = I(t)$.

Therefore,

$$\frac{dS(t)}{dt} + \left(\frac{\beta_d \epsilon(t)}{\rho(t)} + \beta_e\epsilon(t) + \mu_c\right) S(t) = \Delta + \frac{\alpha\epsilon(t)}{1 + b\epsilon(t)}. \tag{3}$$

Here, the integrating factor: $\exp\left(\int_0^t \left(\frac{\beta_d\epsilon(t)}{\rho(t)} + \beta_e\epsilon(t) + \mu_c\right) dt\right) = A$, we can find

$$\int_0^t \left(\frac{d}{dt}[S(t) \times A]\right) dt = \int_0^t \left[\left(\Delta + \frac{\alpha\epsilon(t)}{1 + b\epsilon(t)}\right) \times A\right] dt, \quad (t > 0), \tag{4}$$

which implies

$$S(t)\exp\left(\int_0^t \left(\frac{\beta_d\epsilon(t)}{\rho(t)} + \beta_e\epsilon(t) + \mu_c\right) dt\right) - S^0 = \int_0^t \left[\left(\Delta + \frac{\alpha\epsilon(t)}{1 + b\epsilon(t)}\right) \times A\right] dt. \tag{5}$$

For $S^0 \geq 0$, Eq. (5) indicates the following inequality:

$$S(t) \geq \exp\left(\int_0^t \left(\frac{-\beta_d\epsilon(t)}{\rho(t)} - \beta_e\epsilon(t) - \mu_c\right) dt\right) \times \int_0^t \left[\left(\Delta + \frac{\alpha\epsilon(t)}{1 + b\epsilon(t)}\right) \times A\right] dt. \tag{6}$$

Therefore, $S(t)$ is non-negative for $t > 0$. In the same process, we show that $I(t)$ and $R(t)$ are non-negative for $t > 0$. Hence, the theorem is proved. □

2.1.2. Model boundedness property

Theorem 2. *The system (1) solutions are closed inside the region Π_1 where*

$$\Pi_1 = \left\{(S(t), I(t), R(t)) \in R^3 : \quad N(t) \leq \frac{\Delta}{\mu_c}\right\}_{t\to\infty}$$

Proof. Adding the system Eqs. (1) gives

$$\frac{dN}{dt} = \Delta - \mu_c N - \mu_v I \leq \Delta - \mu_c N. \tag{7}$$

Integrating Eq. (7) and we get

$$N(t) \leq N_0\left(e^{-\mu_c t}\right) + \frac{\Delta}{\mu_c}\left(1 - e^{-\mu_c t}\right). \tag{8}$$

Now, taking lim sup as $t \to \infty$ on (8) and we have

$$\lim_{t\to\infty} N(t) \leq \frac{\Delta}{\mu_c}. \tag{9}$$

Hence, the proof of the theorem is done. □

2.1.3. Disease-free equilibrium E_0

Consider $S'(t) = I'(t) = R'(t) = 0$, in the system (1) to find the disease-free equilibrium point as follows [26]:

$$\begin{aligned} \Delta - \frac{\beta_d SI}{S + I} - \beta_e SI - \mu_c S + \frac{\alpha I}{1 + bI} &= 0, \\ \frac{\beta_d SI}{S + I} + \beta_e SI - \frac{\alpha I}{1 + bI} - (\mu_c + \mu_v + \gamma)I &= 0, \\ \gamma I - \mu_c R &= 0. \end{aligned} \tag{10}$$

Considering $I = 0$ (when there is no infection), we can find the solution of the system (10) as a disease-free equilibrium point as follows:

$$E_0 = (S, I, R) = \left(\frac{\Delta}{\mu_c}, 0, 0\right), \tag{11}$$

Remark 1. If the system reaches the disease-free equilibrium point E_0, the disease disappears from the system and all populations only belong to the susceptible compartment.

2.1.4. The basic reproduction number R_0

In classical epidemiology, the basic reproduction number is an important indicator of the analytical model, denoted as R_0 [27]. R_0 is a threshold defined by the expected average number of new infections generated by one infected person in a fully susceptible population during the period of infection. Using the next generation matrix [28], the basic reproduction number of the system (1) can be considered as follows:

Let, $X = (I(t), S(t))$, then from system (1),

$$\frac{dX}{dt} = \Theta(X) - \Phi(X), \tag{12}$$

where, $\Theta = (F_1, F_2)^T$, $\Phi = (V_1, V_2)^T$, and

$$\begin{pmatrix} \dot{I} \\ \dot{S} \end{pmatrix} = \begin{pmatrix} \frac{\beta_d SI}{S+I} + \beta_e SI \\ 0 \end{pmatrix} - \begin{pmatrix} \frac{\alpha I}{1+bI} + (\mu_c + \mu_v + \gamma)I \\ -\Delta + \frac{\beta_d SI}{S+I} + \beta_e SI + \mu_c S - \frac{\alpha I}{1+bI} \end{pmatrix}. \tag{13}$$

Consider, $E^* = (0, \frac{\Delta}{\mu_c})$ and F, V be the following sub-matrices of the Jacobian of the above system. We obtain

$$F = \left(\frac{\partial \Theta}{\partial X}_{E^*}\right) = \beta_d \mu_c + \Delta\beta_e, \quad \text{and} \quad V = \left(\frac{\partial \Phi}{\partial X}_{E^*}\right) = \mu_c(\alpha + \mu_c + \mu_v + \gamma).$$

The spectral radius of FV^{-1} is equal to R_0. Thus, the basic reproduction number of the system (1) is

$$R_0 = \frac{\beta_d \mu_c + \Delta\beta_e}{\mu_c(\alpha + \mu_c + \mu_v + \gamma)}. \tag{14}$$

Putting the indirect parameter $\beta_e = 0$ in Eq. (14) and we get only direct transmission basic reproduction number R_0^* as follows:

$$R_0^* = \frac{\beta_d}{(\alpha + \mu_c + \mu_v + \gamma)} < R_0. \tag{15}$$

Remark 2. Since the indirect transmission cases increase the basic reproduction number, when we reduce the indirect transmission cases, the basic reproduction number also decreases.

2.2. Stability analysis

In this subsection, we have analyzed the proposed model's local and global stability. Since the first two equations of the system (1) do not relate to $R(t)$, reduce the system (1) as follows:

$$\begin{aligned} \frac{dS}{dt} &= \Delta - \frac{\beta_d SI}{S+I} - \beta_e SI - \mu_c S + \frac{\alpha I}{1+bI} = f_1(S, I), \qquad S(0) = S^0 \\ \frac{dI}{dt} &= \frac{\beta_d SI}{S+I} + \beta_e SI - \frac{\alpha I}{1+bI} - (\mu_c + \mu_v + \gamma)I = f_2(S, I), \quad I(0) = I^0. \end{aligned} \tag{16}$$

We note that two equilibrium points appear in this system (16) as disease-free and endemic equilibrium. A disease-free equilibrium is reached when the basic reproduction number is less than one, and an endemic equilibrium is reached when the basic reproduction number is greater than one [29].

2.2.1. Local stability analysis

For local stability analysis, we first find the Jacobian matrix of the system (16) as follows:

$$J = \begin{pmatrix} -I\left(\frac{\beta_d I}{(S+I)^2} + \beta_e\right) - \mu_c & -S\left(\frac{\beta_d S}{(S+I)^2} + \beta_e\right) + \frac{\alpha}{(1+bI)^2} \\ I\left(\frac{\beta_d I}{(S+I)^2} + \beta_e\right) & S\left(\frac{\beta_d S}{(S+I)^2} + \beta_e\right) - \frac{\alpha}{(1+bI)^2} - (\mu_c + \mu_v + \gamma) \end{pmatrix}. \tag{17}$$

Theorem 3. *The system (16) is locally asymptotically stable at point E_0 if and only if $R_0 < 1$.*

Proof. Here, the diseases-free equilibrium point of system (16) is $E_0\left(\frac{\Delta}{\mu_c}, 0\right)$ and the Jacobian matrix of (17) is

$$J(E_0) = \begin{pmatrix} -\mu_c & \alpha - \beta_d - \frac{\Delta\beta_e}{\mu_c} \\ 0 & \beta_d + \frac{\Delta\beta_e}{\mu_c} - (\alpha + \mu_c + \mu_v + \gamma) \end{pmatrix}. \tag{18}$$

The eigenvalues of Eq. (18) are $\lambda_1 = -\mu_c$, and $\lambda_2 = (\alpha + \mu_c + \mu_v + \gamma)(R_0 - 1)$. Thus, all eigenvalues of J_0 are negative if and only if $R_0 < 1$. Hence, Theorem 3 is proved. □

We have now analyzed the existence of endemic equilibrium at the point $E_1(S, I)$ in the proposed COVID-19 SIR model. Consider $f_1(S, I) = 0$ and $f_2(S, I) = 0$ for the system (16) and rewrite the given system as follows:

$$\begin{aligned} \frac{\beta_d SI}{S+I} + \beta_e SI - \frac{\alpha I}{1+bI} &= \Delta - \mu_c S, \\ \frac{\beta_d SI}{S+I} + \beta_e SI - \frac{\alpha I}{1+bI} &= (\mu_c + \mu_v + \gamma)I, \end{aligned} \tag{19}$$

which implies that

$$\Delta - \mu_c S = (\mu_c + \mu_v + \gamma)I,$$

or,

$$S = \frac{\Delta - (\mu_c + \mu_v + \gamma)I}{\mu_c}. \tag{20}$$

Substituting the value of S into the system's (19) second equation, we get

$$a_1 I^3 + a_2 I^2 + a_3 I + a_4 = 0, \tag{21}$$

where the coefficient values are

$$\begin{cases} a_1 = \beta_e b(\mu_v + \gamma)(\mu_c + \mu_v + \gamma), \\ a_2 = \Delta\mu_c\beta_e b + (\mu_c + \mu_v + \gamma)[b\mu_c(\mu_v + \gamma + \beta_d) + \beta_e(\mu_v + \gamma - 2\Delta b)], \\ a_3 = \mu_c(\mu_v + \gamma)(\alpha + \mu_c + \mu_v + \gamma) - (\mu_c + \mu_v + \gamma)(\Delta\mu_c b + \beta_d\mu_c + 2\Delta\beta_e) \\ \quad +\Delta(\mu_c\beta_e + \mu_c\beta_d b + \Delta\beta_e b), \\ a_4 = \Delta\mu_c(\alpha + \mu_c + \mu_v + \gamma)(R_0 - 1). \end{cases} \tag{22}$$

Here, the coefficient a_1 is always positive and the sign of a_4 depends only on the value of R_0. We are going to discuss the nature of the roots of Eq. (21) for the case $a_1 > 0$. Consider the left-hand side of Eq. (21) as:

$$G(I) = a_1 I^3 + a_2 I^2 + a_3 I + a_4. \tag{23}$$

Differentiating (23) with respect to I, we get

$$\dot{G}(I) = 3a_1 I^2 + 2b_1 I + a_3. \tag{24}$$

Putting $\dot{G}(I) = 0$, we can find

$$I_{1,2} = \frac{-a_2 \pm \sqrt{a_2^2 - 3a_1 a_3}}{3a_1}, \quad D = a_2^2 - 3a_1 a_3. \tag{25}$$

From the above expression we can conclude as follows:

1. If $D > 0$ and $G(I_1)G(I_2) < 0$, then roots are real and different.
2. If $D > 0$ and $G(I_1)G(I_2) > 0$, then only one root is real and two roots are imaginary.
3. If $D > 0$ and $G(I_1)G(I_2) = 0$, then roots are real and two roots are repeated.
4. If $D = 0$ and $G(I_1)G(I_2) = 0$, then three repeated real roots.
5. If $D < 0$, then one root is real and two roots are imaginary.

Therefore, if $R_0 < 1$, then the system (16) has an endemic equilibrium. Later we get the positive endemic state condition in the backward bifurcation subsection.

2.2.2. Global stability analysis

Theorem 4. *The point E_0 is globally asymptotically stable if $R_0 < 1$.*

Proof. First, we consider a Lyapunov function as follows [30]:

$$L = S - \frac{\Delta}{\mu_c} - \frac{\Delta}{\mu_c} ln\left(\frac{\mu_c S}{\Delta}\right) + I, \tag{26}$$

which implies that

$$\frac{dL}{dt} = \frac{\partial L}{\partial S}\frac{dS}{dt} + \frac{\partial L}{\partial I}\frac{dI}{dt} = \left(1 - \frac{\Delta}{\mu_c S}\right)\frac{dS}{dt} + \frac{dI}{dt}. \tag{27}$$

Combining the system (16) and Eq. (26), we get

$$\begin{aligned} \frac{dL}{dt} =& \delta - \mu_c S - (\mu_c + \mu_v + \gamma)I - \left(1 - \frac{\Delta}{\mu_c S}\right) \times \\ & \left(\Delta - \frac{\beta_d SI}{S + I} - \beta_e SI - \mu_c S + \frac{\alpha I}{1 + bI}\right) \\ =& -\frac{1}{\mu_c S}(\Delta - \mu_c S)^2 - I\left(\mu_c + \mu_v + \gamma - \frac{\beta_d \Delta}{\mu_c(S + I)} - \frac{\beta_e \Delta}{\mu_c} - \frac{\Delta\alpha}{\mu_c(1 + bI)}\right). \end{aligned} \tag{28}$$

Thus, we have $\frac{dL}{dt} < 0$ if $R_0 \leq 0$ for all $(S, I) \neq (S^0, 0)$. Also, $\frac{dL}{dt} = 0$ if and only if $(S, I) = (S^0, 0)$. Hence, the La Salle invariance principle states that the point E_0 of the system (16) is globally asymptotically stable. □

3. Bifurcation

In a dynamical system, bifurcation occurs when small, smooth changes in the system's parameter values cause sudden "qualitative" or topological changes in its behavior. Local and global are two types of branches that exist in epidemiology. Common bifurcation types are shown as saddle–node bifurcation or tangent, transcritical bifurcation, pitchfork bifurcation, presented in one-dimensional systems. Bifurcation in two dimensions are basically as tangent, transcritical and Hopf bifurcations. In this section, we analyze the system (16) transcritical, forward, backward and Hopf bifurcations.

3.1. Transcritical bifurcation

By using Sotomayor's theorem for local bifurcations, we want to show that the system (16) has transcritical bifurcations. Define the Jacobian matrix (18) can be calculated as $J = Df(E_0, \beta_d^*)$

$$J = \begin{pmatrix} -\mu_c & -(\gamma + \mu_c + \mu_v) \\ 0 & 0 \end{pmatrix}, \tag{29}$$

where,

$$\beta_d^* = \frac{\mu_c(\alpha + \gamma + \mu_c + \mu_v) - \Delta\beta_e}{\mu_c}, \quad \text{and} \quad R_0 = 1. \tag{30}$$

Here, the eigenvalue of (29) λ_1 is negative and λ_2 is zero for $I = 0$. Calculate right and left eigenvectors as follows:

1. The right eigenvector: $[x_1 \quad x_2]^T$, where $x_1 = \frac{-(\mu_c+\mu_v+\gamma)x_2}{\mu_c}$, $x_2 = x_2$.
2. The left eigenvector: $[y_1 \quad y_2]$, where $y_1 = 0$, $y_2 = y_2$.

Now the system (16) can be written as in a vector form

$$\frac{dY}{dt} = f(Y) \tag{31}$$

where, $Y = (S, I)^T$ and $f = (f_1, f_2)^T$. Find $\frac{df}{d\beta_d}$, we obtain

$$f_{\beta_d} = \left(-\frac{SI}{S+I} \quad \frac{SI}{S+I}\right)^T$$

Which implies

$$f_{\beta_d}(E_0, \beta_d^*) = \begin{pmatrix} 0 & 0 \end{pmatrix}^T.$$

Then

$$\begin{pmatrix} 0 & y_2 \end{pmatrix}.f_{\beta_d}(E_0, \beta_d^*) = 0,$$

$$Df_{\beta_d}(E_0, \beta_d^*) = \begin{pmatrix} 0 & -1 \\ 0 & 1 \end{pmatrix}.$$

Finally, we obtain

$$\begin{pmatrix} 0 & y_2 \end{pmatrix}.\left(Df_{\beta_d}(E_0, \beta_d^*).\left(\frac{-(\mu_c+\mu_v+\gamma)x_2}{\mu_c} \quad x_2\right)^T\right) = -x_2y_2 \neq 0. \tag{32}$$

Thus, according to the Sotomayor theorem, we get the following theorem:

Theorem 5. *The transcritical bifurcation of the system (16) occurs at E_0 when the parameter β_d passes through the bifurcation parameter β_d^*.*

3.2. Backward bifurcation

Considering $\beta_d^* = \beta_d$ as the bifurcation parameter, Eqs. (14) and (26) can be written as :

$$\beta_d^* = \frac{R_0\mu_c(\alpha + \gamma + \mu_c + \mu_v) - \Delta\beta_e}{\mu_c}, \tag{33}$$

$$G^*(I) = a_1^*I^3 + a_2^*I^2 + a_3^*I + a_4^* = 0, \tag{34}$$

where a_1^*, a_2^*, a_3^* and a_4^* are constants.

As follows, find the slope of Eq. (33) with respect to R_0, considering $I = 0$ and $R_0 = 1$:

$$\frac{\partial I}{\partial R_0} = \frac{\Delta\mu_c(\alpha + \mu_c + \mu_v + \gamma)}{\mu_c^2(\alpha + \mu_c + \mu_v + \gamma) + \Delta\beta_e(\mu_v + \gamma) - \Delta b\alpha\mu_c}. \tag{35}$$

Value of Eq. (34) is negative if

$$b > b^{\dagger} = \frac{\mu_c^2(\alpha + \mu_c + \mu_v + \gamma) + \Delta\beta_e(\mu_v + \gamma)}{\Delta\mu_c\alpha}. \tag{36}$$

Hence, we conclude the following theorem.

Theorem 6. *At point $R_0 = 1$, the system (16) consists of a backward bifurcation if $b > b^{\dagger}$.*

Theorem 7. *The point E_1 of the system (16) is a positive endemic state that exists if $b < b^{\dagger}$.*

We have already proved Theorem 7 in 2.2 stability analysis.

3.3. Forward bifurcation

Theorem 8. *A forward bifurcation occurs for the system (16) if $b < b^{\dagger}$ and $R_0 = 1$, where*

$$b^{\dagger} = \frac{\mu_c^2(\alpha + \mu_c + \mu_v + \gamma) + \Delta\beta_e(\mu_v + \gamma)}{\Delta\mu_c\alpha}. \tag{37}$$

Proof. Consider the system (16) as follows:

$$\begin{aligned} h_1 &= \Delta - \frac{\beta_d SI}{S+I} - \beta_e SI - \mu_c S + \frac{\alpha I}{1+bI}, \\ h_2 &= \frac{\beta_d SI}{S+I} + \beta_e SI - \frac{\alpha I}{1+bI} - (\mu_v + \mu_c + \gamma)I. \end{aligned} \tag{38}$$

Taking β_d as a bifurcation parameter and $R_0 = 1$ in Eq. (14) and putting the value of β_d^* in Eq. (18), we can find the eigenvalues of the Jacobian matrix as: $\lambda_1 = -\mu_c$ and $\lambda_2 = 0$. Thus, the assumption of E^* of Theorem 1 in [31] is verified.

Let a_5 and a_6 be the coefficients of the normal form of a system in the central manifold. Calculate the right and left eigenvector for λ_2 as follows:

1. The right eigenvector: $[w_1 \quad w_2]^T$, where $w_1 = \frac{-(\mu_c+\mu_v+\gamma)w_2}{\mu_c}$, $w_2 = w_2$.
2. The left eigenvector: $[v_1 \quad v_2]$, where $v_1 = 0$, $v_2 = v_2$.

The coefficients a_5 and a_6 defined by Theorem 1 in [31] are

$$a_5 = \sum_{k,i,j=1}^{n} v_k w_i w_j \frac{\delta^2 f_k}{\delta x_i \delta x_j}(0,0), \qquad a_6 = \sum_{k,i,j=1}^{n} v_k w_i \frac{\delta^2 f_k}{\delta x_i \delta \phi}(0,0).$$

Since $v_1 = 0$, we can calculate the second partial derivative of f_2 as follows:

$$\frac{\partial^2 f_2}{\partial S^2} = 0, \frac{\partial^2 f_2}{\partial S \partial I} = \frac{\partial^2 f_2}{\partial I \partial S} = \beta_e, \frac{\partial^2 f_2}{\partial I^2} = 2\left(\frac{\Delta b\alpha - \mu_c\beta_d}{\Delta}\right),$$

$$\frac{\partial^2 f_2}{\partial S \partial \beta_d} = 0, \quad \frac{\delta^2 f_2}{\partial I \delta \beta_d} = 1.$$

Thus, we have

$$\begin{aligned} a_5 &= v_2\left(w_1 w_1 \frac{\partial^2 f_2}{\partial S^2} + w_1 w_2 \frac{\partial^2 f_2}{\partial S \partial I} + w_2 w_1 \frac{\partial^2 f_2}{\partial I \partial S} + w_2 w_2 \frac{\partial^2 f_2}{\partial I^2}\right), \\ &= 2v_2 w_2^2\left(\frac{\Delta b\alpha\mu_c - \Delta\beta_e(\mu_v+\gamma) - \mu_c^2(\alpha+\gamma+\mu_c+\mu_v)}{\Delta\mu_c}\right), \\ a_6 &= v_2 w_1 \frac{\partial^2 f_2}{\partial S \partial \beta_d} + v_2 w_2 \frac{\partial^2 f_2}{\partial I \partial \beta_d} = v_2 w_2. \end{aligned}$$

It can be seen that a_6 is always positive and a_5 is positive if

$$b > b^{\dagger} = \frac{\mu_c^2(\alpha + \mu_c + \mu_v + \gamma) + \Delta\beta_e(\mu_v + \gamma)}{\Delta\mu_c\alpha}. \tag{39}$$

Therefore, at $R_0 = 1$, then system (16) undergoes a forward bifurcation when $b < b^{\dagger}$. Hence, the proof of Theorem 7 is done. □

3.3.1. Hopf bifurcation

The proposed COVID-19 SIR model has a Hopf bifurcation if the system (16) contains a pair of complex conjugate eigenvalues of the Jacobian matrix at the equilibrium point. We consider β_d as a bifurcation parameter and the existence of Hopf's bifurcation theorem [32] as follows:

In $\Pi_2 = \{(S(t), I(t)) : S \geq 0, I \geq 0\}$, the system (16) can be converted by

$$\begin{cases} \dot{S} = \Delta(1+bI) - \beta_d SI\left(\frac{1+bI}{N}\right) - \beta_e SI(1+bI) - \mu_c S(1+bI) + \alpha I, \\ \dot{I} = \left(\frac{1+bI}{N}\right) + \beta_e SI(1+bI) - \alpha I - \xi I(1+bI), \end{cases} \tag{40}$$

where

$$\tau = \int_0^t \frac{1}{1+bI}\, dI\ , \quad N = (S+I), \quad \xi = (\mu_c + \mu_v + \gamma)\ :$$

$\dot{S}$ and $\dot{I}$ denote the derivative with respect to the new time variable τ.

Considering $x = S - S^*$, $y = I - I^*$ and convert the system (40) as follows:

$$\begin{cases} \dot{x} = a_7 x + a_8 xy + a_9 y + a_{10} y^2 + a_{11} xy^2, \\ \dot{y} = a_{12} x + a_{13} xy + a_{14} y + a_{15} y^2 + a_{16} xy^2, \end{cases} \tag{41}$$

where the coefficients are

$$\begin{cases} a_7 = -\left(\frac{\beta_d I^*}{N} + \beta_e I^* + \beta_e b I^{*^2} + \mu_c + \mu_c b I^*\right), \\ a_8 = -\left(\frac{\beta_d}{N} + \beta_e + \beta_e b I^* + \beta_e b + \mu_c b\right), \\ a_9 = \left(\Delta b - \frac{\beta_d S^*}{N} - 2\frac{\beta_d b S^* I^*}{N} - \beta_e S^* - 2\beta_e b S^* I^* - \mu_c S^* b + \alpha\right), \\ a_{10} = -\left(\frac{\beta_d b S^*}{N} + \beta_e b S^*\right), \\ a_{11} = -\left(\frac{\beta_d b}{N} + \beta_e b\right), \\ a_{12} = \left(\frac{\beta_d I^*}{N} + \frac{\beta_d b I^{*2}}{N} + \beta_e I^* + \beta_e b I^{*2}\right), \\ a_{13} = \left(\frac{\beta_d}{N} + 2\frac{\beta_d b I^*}{N} + \beta_e + 2\beta_e b I^*\right), \\ a_{14} = \left(\frac{\beta_d S^*}{N} + 2\frac{\beta_d b S^* I^*}{N} + \beta_e S^* + 2\beta_e b S^* I^* - \alpha - \xi - 2\xi b I^*\right), \\ a_{15} = \left(\beta_e b - \frac{\beta_d b S^*}{N} - \xi b\right), \\ a_{16} = -\left(\frac{\beta_d b}{N} + \beta_e b\right), \end{cases} \tag{42}$$

when

$$\Delta - \frac{\beta_d S^* I^*}{N} - \frac{\beta_d b S^* I^{*2}}{N} - \beta_e S^* I^* - \beta_e b S^* I^{*2} - \mu_c S^* + \alpha I^* = 0,$$
$$\frac{\beta_d S^* I^*}{N} + \frac{\beta_d b S^* I^{*2}}{N} + \beta_e b S^* I^{*2} - \alpha I - \xi I^* - \xi b I^{*2} = 0.$$

Suppose $\beta_d = \beta_d^*$, then according to (18) we obtain

$$\mathrm{tr}(J(E_0)) = -\mu_c, \qquad \text{and} \qquad \det(J(E_0)) = \mu_c^2.$$

Thus, we have

$$\mathrm{tr}^2(J(E_0)) < 4\det(J(E_0)), \tag{43}$$

which implies the following theorem [33]:

Theorem 9. *The system (16) exists hopf bifurcation at equilibrium point E_0 and $b = b^\dagger = \frac{\mu_c^2(\alpha+\mu_c+\mu_v+\gamma)+\Delta\beta_e(\mu_v+\gamma)}{\Delta\mu_c\alpha}$, when bifurcation parameter β_d passes through the critical value*

$$\beta_d^* = \frac{2}{\pi}\arctan\left(\frac{\sqrt{|tr^2(J(x^*,y^*)) - 4\det(J(x^*,y^*))|}}{tr(J(x^*,y^*))}\right)$$

if $tr^2(J(x^*,y^*)) - 4\det(J(x^*,y^*)) < 0$ *and* $tr(J(x^*,y^*)) > 0$.

3.4. Numerical simulation of bifurcations

In this subsection, we numerically show forward, backward, transcritical, and Hopf bifurcations of the system (16). Since our main focus is to analyze the bifurcation and implement control variables with the model to mitigate COVID-19, for simulation purposes, we use parameter values from some references and estimated values indicated in Table 1.

3.4.1. Transcritical bifurcation

Using the MATCONT software and Table 1 parameter values with $b = 0.0008$, we plot the transcritical bifurcation. Here the branch point $\beta_d^* = 1.023$, red and black curves represent unstable and stable states, respectively. In biology, when $\beta_d^* < 1.023$, the stable disease-free equilibrium is zero, which means that the species cannot survive. Similarly, when $\beta_d^* > 1.023$, the stable disease-free equilibrium is greater than zero, which means that the population remains unchanged. Fig. 2(b) shows the vector field of the transcritical bifurcation.

Table 1
Description and estimation of the model parameter values for bifurcation analysis.

Parameters	Description	Estimated value	References
β_d	Direct transmission rate	1.023	Assumed
Δ	Recruitment rate	7.46	Assumed
β_e	Indirect transmission rate	0.001	Assumed
α	Cure rate	1	Assumed
μ_c	Natural death rate	0.02	[34]
μ_v	Death rate due to diseases	0.1	[34]
γ	Natural recovery rate	0.003	[35]
N	Total number of population	100	[36]

Table 2
Sensitivity indices of R_0 for the parameter values of bifurcation analysis.

Parameters	Description	Sensitivity index (R_0)
β_d	Direct transmission rate	+0.733
Δ	Recruitment rate	+0.267
β_e	Indirect transmission rate	+0.267
α	Cure rate	−0.890
μ_c	Natural death rate	−0.285
μ_v	Death rate due to diseases	−0.089
γ	Natural recovery rate	−0.003

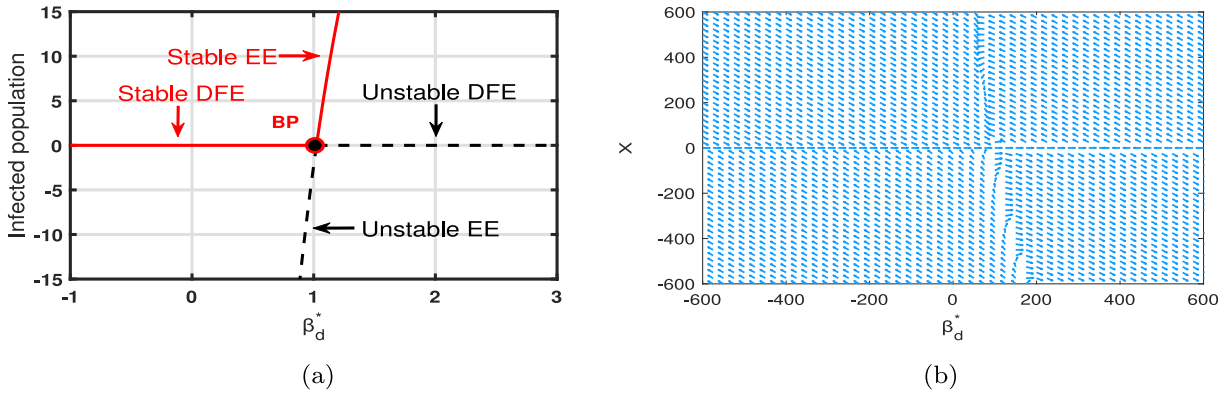

Fig. 2. The transcritical bifurcation of system (16) exists when $b = 0.0008$. (a) For transcritical, the branch point (BP) value is $\beta_d^* = 1.023$. Red and black curves indicate disease-free equilibrium (DFE) and local equilibrium (EE), while dotted and solid lines indicate unstable and steady state, respectively; (b) Vector field diagram.

3.4.2. Forward bifurcation

By Theorem 8, if $b < b^\dagger$, the system (16) is a forward bifurcation. Using these parameter values from Table 1, we get $b^\dagger = 8\times10^{-3}$. Considering the value of $b = 8 \times 10^{-4} < b^\dagger$ as the mentioned Theorem 8, we draw a dynamic graph using MATCONT, which is the forward bifurcation illustration. From Fig. 3(a), we conclude a result that the system (16) has a stable disease-free equilibrium when $\beta_d^* < 1.023$ $\left(R_{0(\beta_d=1.023)} = 1\right)$ and an unstable disease-free equilibrium when the value of β_d^* increases. Also, the stable endemic equilibrium point starts at $\beta_d^* = 1.023$ and increasing the value of β_d^*, the curve of endemic equilibrium also moves forward and the state is stable. Biologically, the long-term behavior of the model only depends on whether R_0 is greater or less than 1, which means that the system (16) is robust in the initial conditions.

3.4.3. Backward bifurcation:

By Theorem 5, if $b > b^\dagger$, the system (16) has a backward bifurcation. In the former forward bifurcation part, we get $b^\dagger = 8\times10^{-3}$. Considering the value of $b = 8 \times 10^{-2} > b^\dagger$ in Theorem 5, we draw a dynamic graph Fig. 3(b) using MATCONT, which is the backward bifurcation illustration. From the figure, we conclude a result that the system (16) has a stable disease-free equilibrium when $\beta_d^* < 1.023$ and an unstable disease-free equilibrium when the value of β_d^* increases. Also, the unstable endemic equilibrium point starts at $\beta_d^* = 1.023$ and decreasing the value of β_d^* an unstable endemic equilibrium occurs. When the value of $\beta_d^* = 0.494$ which is shown in the curve as the Limit Point (LP), then again endemic equilibrium state stable and increased the value β_d^*, curves move forward and state stable. This phenomenon is known as bistability [37] as it is shown in Fig. 3(b). Biologically, this means that whenever a backward bifurcation occurs, the system (16) is very sensitive to small perturbations in the initial conditions, since it can lead to large differences in the dynamic behavior of the final state of COVID-19.

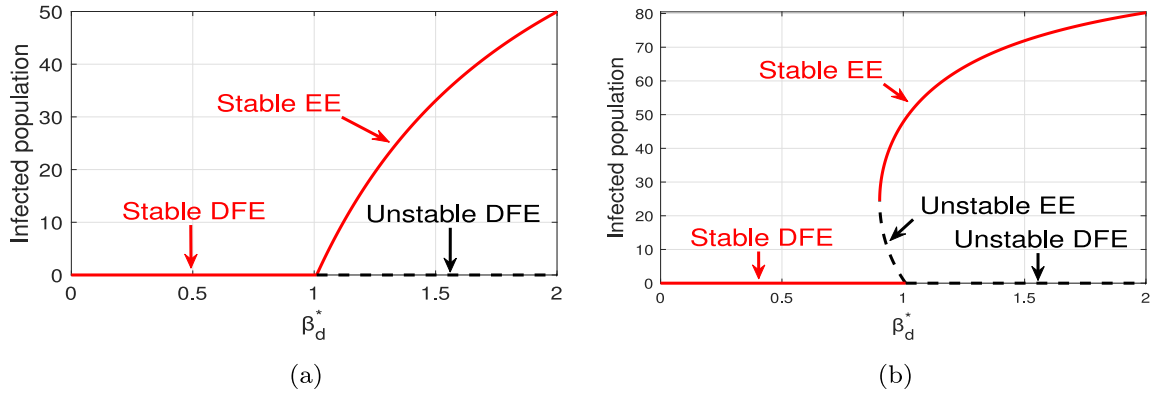

Fig. 3. The dynamical diagram of forward and backward bifurcation. Red and black curves indicate disease-free equilibrium (DFE) and endemic equilibrium (EE), while dotted and solid lines indicate unstable and steady state, respectively; (a) for forward bifurcation $b = 8\times10^{-4}$; (b) for backward bifurcation $b = 8\times10^{-2}$.

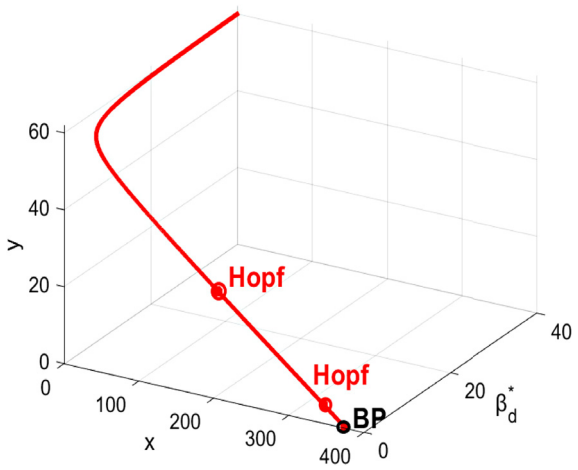

Fig. 4. Dynamical behavior of two Hopf (H) bifurcation when $b = b^{\dagger}$..

3.4.4. Hopf bifurcation

Earlier we show that the system (16) exists Hopf bifurcation. By Theorem 9, if $b = b^{\dagger}$, the system (16) exists two Hopf bifurcations when using all parameter values of Table 1. With MATCONT we draw a dynamic graph. Fig. 4 represents two Hopf bifurcations. The first Hopf bifurcation occurs at the point $x = 344.23$, $y = 4.67$ and the bifurcation parameter value $\beta_d^* = 0.216$ is shown in Fig. 5(a). Fig. 5(b) represents another Hopf bifurcation with values $x = 202.95$, $y = 27.65$ and bifurcation parameter value $\beta_d^* = 0.364$. Mathematically, we know that the Hopf bifurcation is the critical point where the stability of the system switches and a periodic solution emerges. Biologically speaking, the existence of Hopf bifurcation indicates that disease can survive in a community, which is a potentially critical situation for governments to control the spread of disease.

3.5. Preliminary conclusions

Our proposed COVID-19 SIR model is positive and bounded. We found that if the basic reproduction number $R_0 < 1$ [38], then COVID-19 will disappear and if $R_0 = 1$ [39], then the disease COVID-19 will remain in the system and will remain stable. Also, when the value of R_0 is greater than 1 [40], COVID-19 will spread and cause an outbreak. Our model has forward, backward and Hopf bifurcations. Furthermore, there are stable and unstable disease-free and endemic equilibria on forward and backward bifurcations.

In Fig. 6 three parameters determine how fast and how many people move from one compartment to another. Also, Fig. 7 is the dynamic behavior of cumulative death of the system (1). It represents the total number of deaths over a fixed time period. After increasing time, the number of cumulative death also increases. Our analysis shows that the 35-day system (1) of Fig. 6 has a high infection rate that can occur in both direct and indirect infections. To control this outbreak, we are improving our proposed COVID-19 SIR model by including two control parameters. One control is the use of face masks, hand sanitizer, social distancing [41] and the other is the injection of a vaccine [42] into the human body.

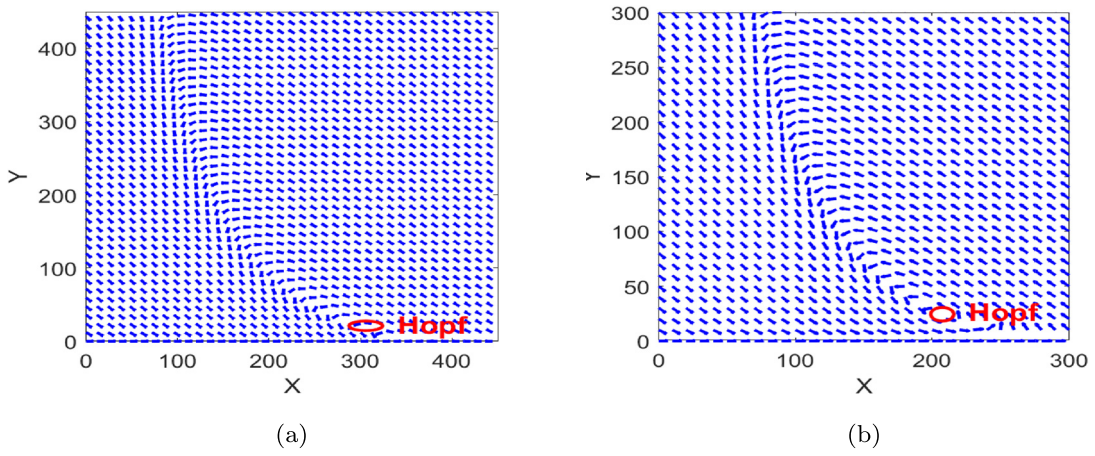

Fig. 5. Two Hopf bifurcation vector fields in the system (16).(a) The first Hopf bifurcation occurs at the point $x = 344.23, y = 4.67$; (b) The 2nd Hopf bifurcation occurs at the point $x = 202.95, y = 27.65$.

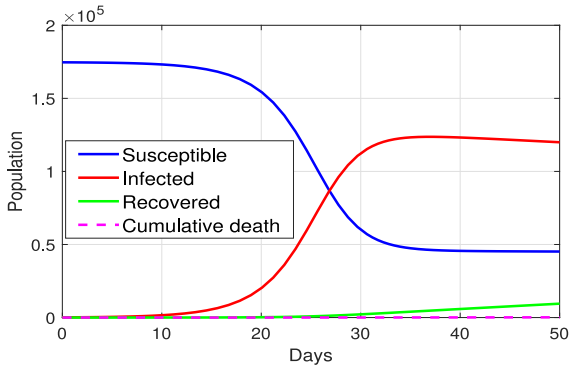

Fig. 6. Dynamic behavior of the susceptible, infected and recovered population of the proposed COVID-19 SIR model.

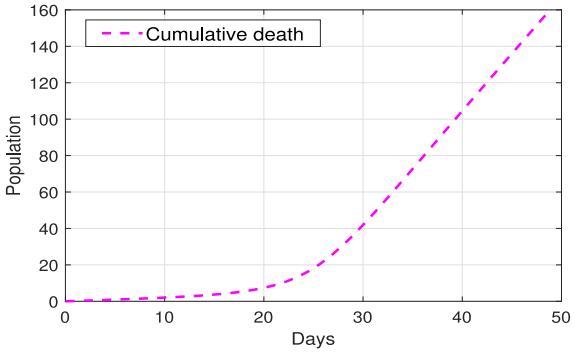

Fig. 7. Dynamic behavior of the cumulative death in the proposed COVID-19 SIR model.

4. An improved model with the control program

To reduce the spread of COVID-19, we use control variables and improved our model. In this paper, we consider two control variables (i) face mask, hand sanitizer, social distancing, and (ii) vaccination. For computational simplicity, we exclude other controls such as immunization (due to natural infection and vaccination), variants, vaccine efficacy, different vaccine brands, multiple doses, antiviral therapy (e.g. Paxlovid), boosters in our paper, and quarantine that will be added in future studies. A description of the controls is as follows:

Table 3
Parameters and initial conditions of the proposed COVID-19 SIR model.

Parameters	Description	Estimated Value	References
β_d	Direct transmission rate	0.75	[34]
Δ	Recruitment rate	0.03	[34]
β_e	Indirect transmission rate	1.5×10^{-10}	Assumed
α	Cure rate	0.5	[20]
μ_c	Natural death rate	1.0×10^{-6}	Assumed
b	Saturation parameter	1.2×10^{-5}	Assumed
μ_v	Death rate due to diseases	5.0×10^{-5}	Assumed
γ	Natural recovery rate	3.0×10^{-3}	[35]
ρ	rate of vaccination of susceptible	0.8	Assumed
S^0	Susceptible individuals	174673	[35]
I^0	Infected individuals	132	[35]
R^0	Recovered individuals	0.00	[25]

(i) **Face masks, hand sanitizer, social distancing:** Health experts strongly recommend surgical masks, not only for infected people but also for susceptible individuals. Many infected people have no symptoms. Use only face masks, hand sanitizer, and social distancing to reduce the spread of COVID-19. In our improved model, we denote face masks, hand sanitizer use, and social distancing control as $u_1(t)$.

(ii) **Vaccination:** Vaccination is one of the important medicines to prevent the spread of COVID-19 disease. The body can produce antibodies to protect against the coronavirus by injecting proper doses of vaccine. In our improved model, we denote only the vaccination control as $u_2(t)$.

Above this control our improved model is as follows:

$$\begin{aligned}
\frac{dS}{dt} &= \Delta - \frac{\beta_d SI}{S+I} - \beta_e SI - \mu_c S + \frac{\alpha I}{1+bI} - (u_1(t) + \rho u_2(t))S, \quad S(0) = S^0, \\
\frac{dI}{dt} &= \frac{\beta_d SI}{S+I} + \beta_e SI - \frac{\alpha I}{1+bI} - (\mu_c + \mu_v + \mu_\gamma)I - u_1(t)I, \quad I(0) = I^0, \\
\frac{dR}{dt} &= u_1(t)(S+I) + \rho u_2(t)S + \gamma I - \mu_c R, \qquad\qquad R(0) = R^0,
\end{aligned} \tag{44}$$

with u_1 and u_2 are positive values.

4.1. Analysis of improved model and the basic reproduction number

In the absence of control strategies, we have already analyzed the positivity and boundedness properties, disease-free equilibrium point, basic reproduction number, and the stability of the system (44) in the previous subsection of 2.1.

4.2. Sensitivity analysis

We apply a sensitivity analysis technique to perform the bifurcation analysis and determine the importance of each model parameter for controlling the COVID-19 viral infection. Here we compute a sensitivity analysis of R_0 for the model parameter [43]. According to the basic reproduction number R_0, the sensitivity index for x_i is calculated as follows:

$$\Lambda_{x_i}^{R_0} = \frac{\partial R_0}{\partial x_i} \times \frac{x_i}{R_0}. \tag{45}$$

Using Eq. (45) above and the values of the parameters in Table 1 and Table 3, evaluate the parameter sensitivity indices of R_0 (see Table 2 and Table 4). As shown in Table 4, a sensitive parameter of the basic reproduction number is the direct infection rate of susceptible to infected individuals, denoted by β_d with a sensitivity index of 1. That is, increasing or decreasing the value of R_0 by 1% it is required to increase or decrease the value of β_d by 1%. Other parameters' sensitivity indices are shown in Table 2 and Table 4 respectively. Our exclusion of data-driven parameter estimates is a limitation of this paper. However, data-driven models will be more useful, making research more relevant and applicable.

4.3. Characterization of the optimal control

In this subsection, we analyze the control model optimality by using the control parameters [42]. Our primary goal is to reduce total COVID-19 transmission and use containment measures to vaccinate susceptible individuals. Increase the face masks, hand sanitizers, and social distancing among susceptible and infected individuals. We consider the objective function as follows:

$$J(u_1, u_2) = \int_0^T \left(b_1 I(t) + \frac{1}{2} w_1 u_1^2 + \frac{1}{2} w_2 u_2^2 \right) dt \,, \tag{46}$$

where b_1 is a positive weight constant for infected individuals and w_1, w_2 are positive weight constants for face masks, hand sanitizer, social distancing, and vaccination, respectively. We choose quadratic cost on control, which is the simplest and most widely used

Table 4
Sensitivity indices of R_0 to the parameter values of the COVID-19 SIR model.

Parameters	Description	Sensitivity index (R_0)
β_d	Direct transmission rate	+1
Δ	Recruitment rate	+0.000006
β_e	Indirect transmission rate	+0.000006
α	Cure rate	−0.9939
μ_c	Natural death rate	−0.00000798
μ_v	Death rate due to diseases	−0.0000993
γ	Natural recovery rate	−0.00596

non-linear representation of control cost. Quadratic terms are specifically chosen to describe the non-linear behavior of the face masks, hand sanitizer, social distancing, and vaccination implementation costs. Here, $w_1u_1^2$ and $w_2u_2^2$ are the cost of face masks, hand sanitizer, social distancing, and vaccination efforts, respectively. Most mathematical models using optimal control theory rely on Pontryagin's maximum principle, which is a first-order condition for finding an optimal solution. This is a powerful method for computing optimal control, and its key advantage is that it does not require prior evaluation of the minimal cost function. Using Pontryagin's Maximum Principle [44], to find the optimal solution of the improved model. To optimal control u_1^* and u_2^*, such that

$$J(u_1^*, u_2^*) = \min_{\Pi_2} J(u_1, u_2), \tag{47}$$

where

$$\Pi_3 = \{u_i |\ 0 \le u_i \le 1,\ \text{Lebesgue measurable }\}. \tag{48}$$

We need the minimal value of Pontryagin's Maximum Principal. For this, the Hamiltonian H, is given by

$$\begin{aligned} H &= b_1 I(t) + \frac{1}{2}w_1u_1^2 + \frac{1}{2}w_2u_2^2 \\ &+ \lambda_1\left(\Delta - \frac{\beta_d SI}{S+I} - \beta_e SI - \mu_c S + \frac{\alpha I}{1+bI} - u_1 S - \rho u_2(t)S\right) \\ &+ \lambda_2\left(\frac{\beta_d SI}{S+I} + \beta_e SI - \frac{\alpha I}{1+bI} - (\mu_c + \mu_v + \mu_\gamma)I - u_1(t)I\right) \\ &+ \lambda_3\left(u_1(S+I) + \rho u_2(t)S + \gamma I - \mu_c R\right). \end{aligned} \tag{49}$$

Theorem 10. *There exists an optimal control u_1^*, u_2^* and the corresponding solution (S^*, I^*, R^*) that minimizes J over Π_2. For the above statement to be true, there exist adjoint functions $\lambda_1(t), \lambda_2(t), \lambda_3(t)$ such that*

$$\begin{aligned} \frac{d\lambda_1}{dt} &= (\lambda_1 - \lambda_2)I^*\left(\frac{\beta_d I^*}{(S^*+I^*)^2} + \beta_e\right) + \lambda_1\mu_c + (u_1^* + \rho u_2^*)(\lambda_1 - \lambda_3), \\ \frac{d\lambda_2}{dt} &= -b_1 + (\lambda_1 - \lambda_2)S^*\left(\left(\frac{\beta_d S^*}{(S^*+I^*)^2} + \beta_e\right) - \frac{\alpha}{(1+bI^*)^2}\right) \\ &\quad + \lambda_2(\mu_c + \mu_v + \gamma) + (\lambda_2 - \lambda_3)u_1^* - \lambda_3\gamma, \\ \frac{d\lambda_3}{dt} &= \lambda_3\mu_c, \end{aligned} \tag{50}$$

with the transversality conditions

$$\lambda_1(T) = 0, \quad \lambda_2(T) = 0, \quad \lambda_3(T) = 0. \tag{51}$$

Also,

$$\begin{aligned} u_1^*(t) &= \min\left(\max\left(0, \frac{(\lambda_1 - \lambda_3)S^* + (\lambda_2 - \lambda_3)I^*}{w_1}\right), 1\right), \\ u_2^*(t) &= \min\left(\max\left(0, \frac{\rho(\lambda_1 - \lambda_3)S^*}{w_2}\right), 1\right). \end{aligned} \tag{52}$$

Proof. From Pontryagin's Maximum Principle, we get:

$$\frac{d\lambda_1}{dt} = -\frac{\delta H}{\delta S}, \qquad \frac{d\lambda_2}{dt} = -\frac{\delta H}{\delta I}, \qquad \frac{d\lambda_3}{dt} = -\frac{\delta H}{\delta R}, \tag{53}$$

with $\lambda_1(T) = 0$, $\lambda_2(T) = 0$, and $\lambda_3(T) = 0$ assessed at the optimal control and which outcomes the adjoint system (50). We differentiate H with respect to u_1^*, u_2^* on the set Π_2, respectively.

$$\begin{aligned} \frac{\delta H}{\delta u_1} &= u_1w_1 - \lambda_1 S - \lambda_2 I + \lambda_3(S+I) = 0, \quad at \quad u_1 = u_1^*, \\ \frac{\delta H}{\delta u_2} &= u_2w_2 - \rho\lambda_1 S + \rho\lambda_3 S = 0, \quad at \quad u_2 = u_2^*. \end{aligned} \tag{54}$$

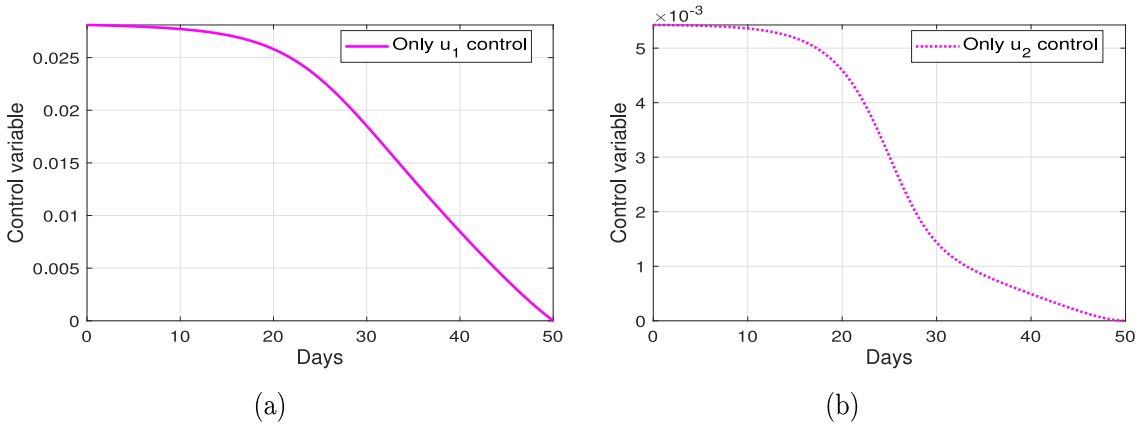

Fig. 8. Dynamic diagram of control variables: (a) optimal control u_1, (b) optimal control u_2.

Solving system (54) for u_1^* and u_2^* we get

$$u_1^* = \frac{(\lambda_1 - \lambda_3)S + (\lambda_2 - \lambda_3)I^*}{w_1},$$
$$u_2^* = \frac{\rho(\lambda_1 - \lambda_3)S^*}{w_2}. \tag{55}$$

Hence, the proof of the theorem is done. □

We use three different control strategies to find the best results. The three strategies are as follows:

(i) **Strategy 1:** Face masks, hand sanitizer, social distancing control on susceptible and infected compartment (control $u_1(t)$ alone).
(ii) **Strategy 2:** Vaccination control on susceptible compartment (control $u_2(t)$ alone).
(iii) **Strategy 3:** Both face masks, hand sanitizer, social distancing control, and vaccination control on susceptible and infected compartments (both controls $u_1(t)$ and $u_2(t)$).

5. Numerical simulations and discussions

In this section, we analyze the numerical solution of the system with optimal control for different cases that have been discussed. To demonstrate the effect of optimal control, we numerically solve the optimal system using the forward–backward sweep method [45]. This method consists of six ordinary differential equations from the state and adjoint equations with two controls. The method combines the forward application of Euler's method to the state system and the backward application of Euler's method to the adjoint system at a time $t \in [0, T]$ and transversality conditions. We choose the control boundaries for u_1, u_2 to be 0 to 1. We use the same method for the result until the convergence condition is reached. We simulate the model in different scenarios.

To find the optimal control problem, we use three control strategies and consider the weight constant parameter values as follows: $C_1 = 2, W_1 = 10^8, W_2 = 10^9$. This paper does not include detailed information on changes in weight constant values, as the results are not very sensitive. The general shapes of the curves are similar, however, the amplitudes vary slightly. As we increase the weight constants and increase the cost of infected constant, the total recovery has increased due to reduced infected individuals.

5.1. *Strategy 1: Only face masks, hand sanitizer, social distancing control* $u_1(t)$

Fig. 8(a) represents the dynamic curve of face masks, hand sanitizer, and social distancing control $u_1(t)$. In Fig. 9(a), Only face masks, hand sanitizer, social distancing control infected population curve begins with the uncontrol infected population curve and remains the same for 10 days. After 10 days, the infection rate decreases slightly due to the effect of face masks, hand sanitizer, social distancing control. Fig. 10(a) shows recovered individuals with and without control of u_1. On the initial day, the u_1 control curve slopes smoothly upward. Over time, the difference between recovered individual curves with and without control increases.

5.2. *Strategy 2: only vaccination control* $u_2(t)$

As can be seen in Fig. 9(b), the infection compartment curve at day 35 is presented as the maximum number of infected persons in the absence of control. Applying only the vaccination control $u_1(t)$ to the COVID-19 SIR model shown in Fig. 8(b), the infection compartment curve in Fig. 9(b) remains with the former (no control) curve. After 22 days the infected curve of vaccination control differs from no control and decreases over time. The effect of vaccination control on recovered individuals is shown in Fig. 10(b). In the beginning, the curve of no control and only vaccination control differ from each other. We see a better result for the recovery curve of vaccination control implementation than for the no-control curve.

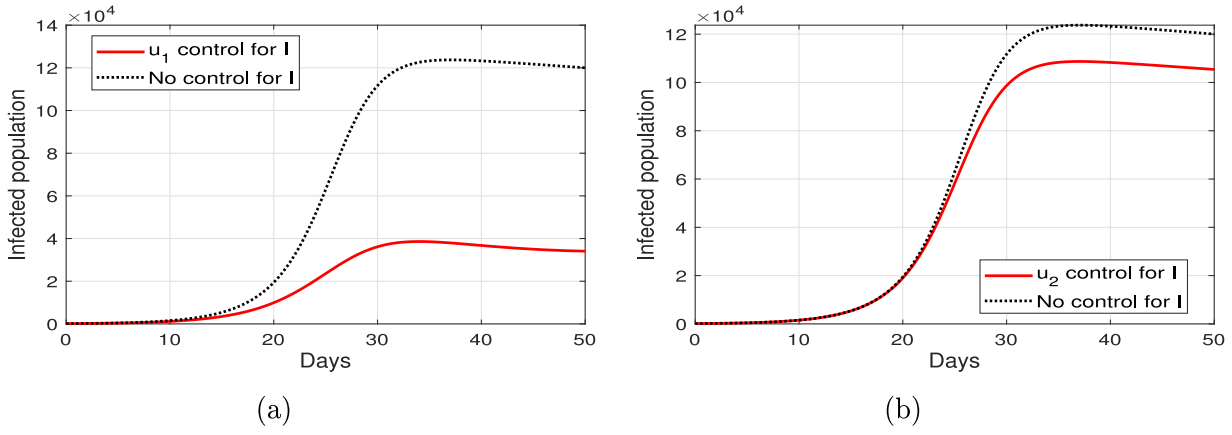

Fig. 9. Dynamic diagram of infected population with and without control: (a) face masks, hand sanitizer, social distancing control u_1, (b) vaccination control variable u_2.

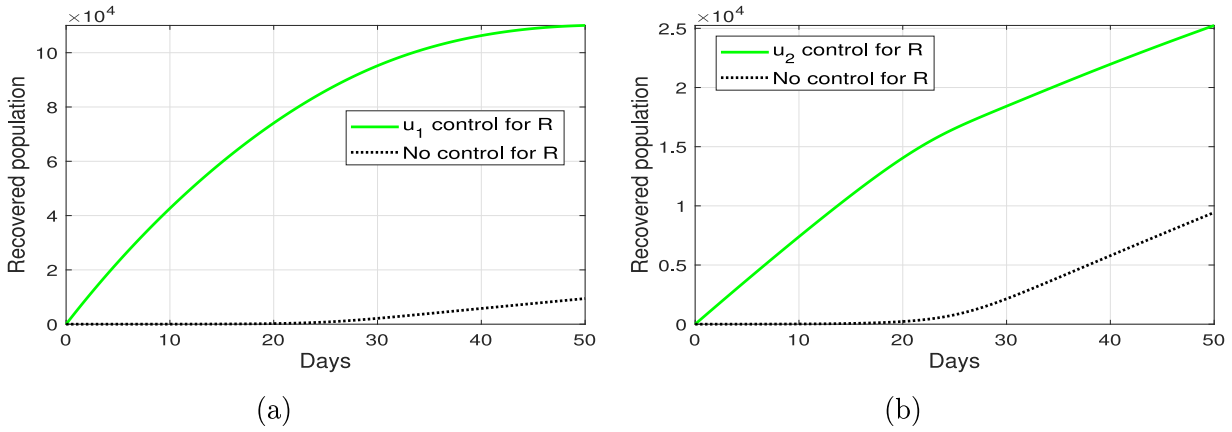

Fig. 10. Dynamic diagram of recovered population with and without control: (a) face masks, hand sanitizer, social distancing control u_1, (b) vaccination control variable u_2.

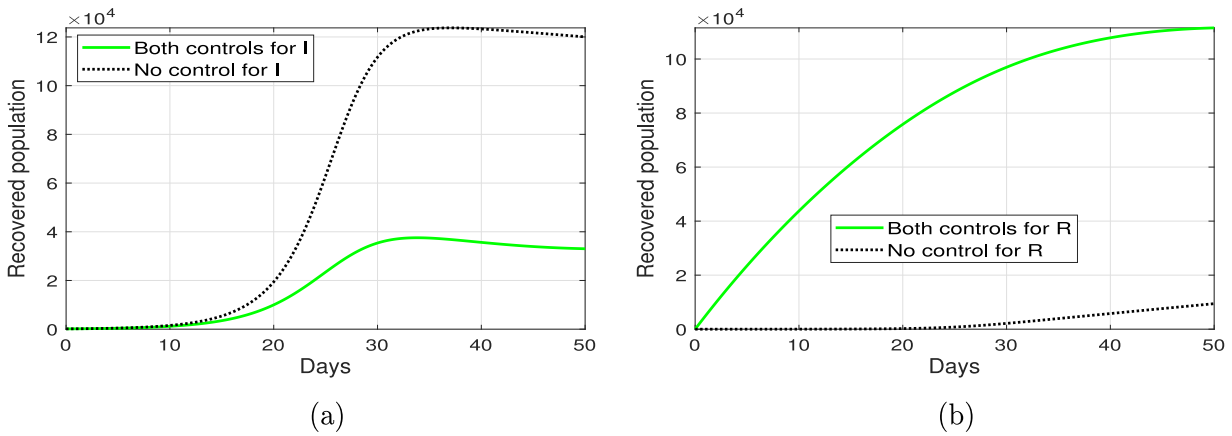

Fig. 11. Dynamic diagram of population both and without control: (a) infected individuals, (b) recovered individuals.

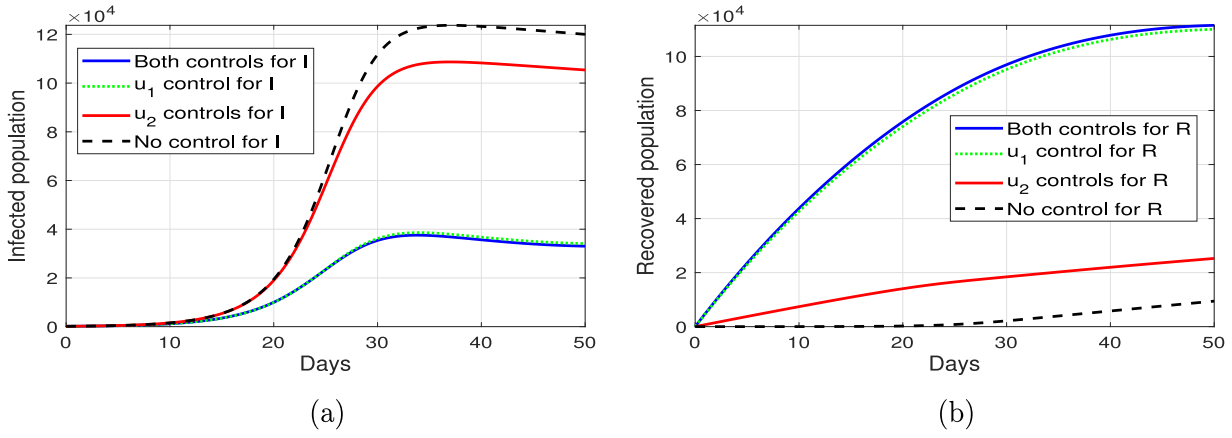

Fig. 12. Comparison of dynamic diagram of control effects of single, both, and without control. (a) Infected population, (b) recovered population.

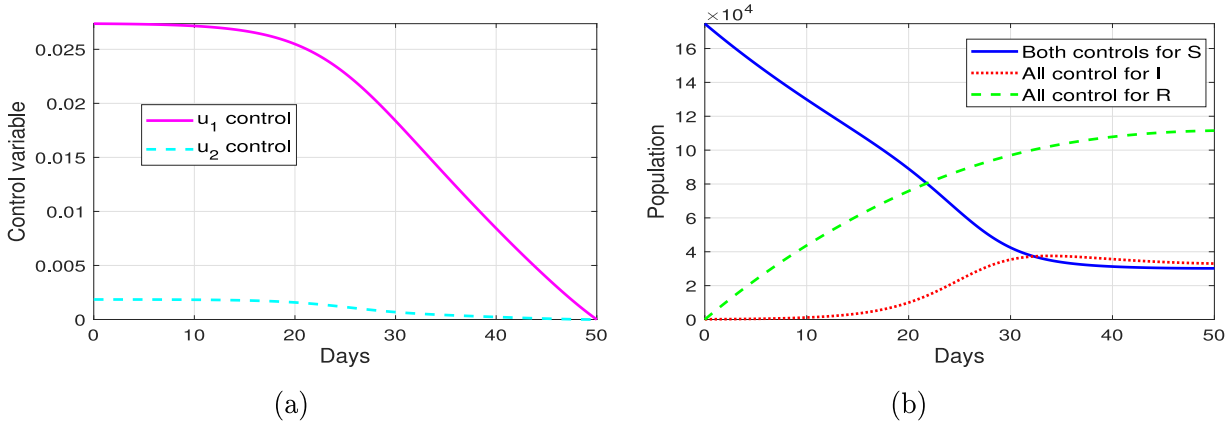

Fig. 13. Dynamic figure of (a) both controls, (b) SIR model with the effect of both controls.

5.3. Strategy 3: both controls $u_1(t)$ and $u_2(t)$.

In Fig. 13(a), the effects of both controls are shown. In Fig. 11(a), we see that when both controls are applied the infected curve decreases from the 10th day compared with no control curve. Recover population individual curves on Fig. 11(b), represent better results between both control and without control recovered curves. However, the rate of recovered individuals shows better for implementing both controls.

5.4. Final observation

Here, we show the results of a comparison of individual controls and both controls. Fig. 12(a) presents a comparison of the dynamic curves of infected individuals for both controls, face masks, hand sanitizer, social distancing control alone, vaccination alone, and without control respectively. Applying the u_2 control reduces infection by approximately 12.21%. Control u_1 shows better results than control u_2 and reduces infection by approximately 71.60%. Finally, when we implemented both controls, reduces infection by approximately 72.50%. Clearly, both controls result in infected individuals doing better than single control.

Fig. 12(b) presents a comparison of the dynamic curves of recovered individuals for both controls, Face masks, hand sanitizer, social distancing alone vaccination alone, and without control respectively. Applying the u_2 control increases recovered by approximately 62.53%. Control u_1 shows better results than control u_2 and increases recovered by approximately 91.01%. Finally, when we implemented both controls, increases recovered by approximately 92.00%. Definitely, both controls result in recovered individuals doing better than single control.

Figs. 13(a) and 13(b) represent the dynamic curve of both controls and the effect of both controls in the proposed COVID-19 SIR model respectively. When both controls are implemented, the number of infected individuals decreases and the number of recovered individuals increases steadily. However, the results are better than the only u_1 and only u_2 control respectively.

6. Conclusion

In this paper, we analyze the COVID-19 SIR model and characterize its positivity and boundness properties. The local and global stability of the disease-free equilibrium point is also discussed along with its biological significance. Furthermore, for the direct transmission parameter β_d, we show that the model has disease-free and endemic equilibrium points. We show that the model has forward, backward, transcritical, and Hopf bifurcations. we introduce two control variables (face masks, hand sanitizer, social distancing and vaccination) with the proposed model and solve an optimal control problem by Pontryagin's maximum principle. Finally, we conclude that optimal control of face masks, hand sanitizer, social distancing control and vaccination in our COVID-19 SIR model can reduce the spread of the disease.

Declaration of competing interest

The authors declare the following financial interests/personal relationships which may be considered as potential competing interests: Mostak Ahmed reports financial support was provided by Jagannath University. Mostak Ahmed reports a relatonship with Jagannath University that includes: employment.

Data availability

No data was used for the research described in the article.

Acknowledgments

The authors would like to thank the University Grants Commission (UGC) of Bangladesh for funding the corresponding author as a post-doctoral fellow.

References

[1] World Health Organization, et al. Naming the coronavirus disease (COVID-19) and the virus that causes it. Brazilian J Implantol Health Sci 2020;2(3).
[2] Mor S, Saini P, Wangnoo SK, Bawa T. Worldwide spread of COVID-19 pandemic and risk factors among co-morbid conditions especially diabetes mellitus in India. Res J Pharmacy Technol 2020;13(5):2530–2.
[3] Cooper I, Mondal A, Antonopoulos CG. A SIR model assumption for the spread of COVID-19 in different communities. Chaos Solitons Fractals 2020;139:110057.
[4] Scarpino SV, Petri G. On the predictability of infectious disease outbreaks. Nature Commun 2019;10(1):1–8.
[5] Chinazzi M, Davis JT, Ajelli M, Gioannini C, Litvinova M, Merler S, et al. The effect of travel restrictions on the spread of the 2019 novel coronavirus (COVID-19) outbreak. Science 2020;368(6489):395–400.
[6] Hasan MM, Ahmed M, Urmy SA. Efficacy of limited antiviral treatment, testing, hospitalization, and social distancing for COVID-19 pandemic. Sens Int 2021;2:100112.
[7] Kucharski AJ, Russell TW, Diamond C, Liu Y, Edmunds J, Funk S, et al. Early dynamics of transmission and control of COVID-19: a mathematical modelling study. Lancet Infect Dis 2020;20(5):553–8.
[8] Masud MAB, Ahmed M, Rahman MH. Optimal control for COVID-19 pandemic with quarantine and antiviral therapy. Sens Int 2021;2:100131.
[9] Kumar RP, Basu S, Santra P, Ghosh D, Mahapatra G. Optimal control design incorporating vaccination and treatment on six compartment pandemic dynamical system. Results Control Optim 2022;7:100115.
[10] Gaeta G. A simple SIR model with a large set of asymptomatic infectives. 2020, arXiv preprint arXiv:2003.08720.
[11] Kaddar A, Abta A, Alaoui HT. A comparison of delayed SIR and SEIR epidemic models. Nonlinear Anal Model Control 2011;16(2):181–90.
[12] Ndaïrou F, Area I, Nieto JJ, Torres DF. Mathematical modeling of COVID-19 transmission dynamics with a case study of Wuhan. Chaos Solitons Fractals 2020;135:109846.
[13] Bakare EA, Nwagwo A, Danso-Addo E. Optimal control analysis of an SIR epidemic model with constant recruitment. Int J Appl Math Res 2014;3(3):273.
[14] Matusik R, Nowakowski A. Control of COVID-19 transmission dynamics, a game theoretical approach. Nonlinear Dynam 2022;110(1):857–77.
[15] Zhang X, Liu X. Backward bifurcation of an epidemic model with saturated treatment function. J Math Anal Appl 2008;348(1):433–43.
[16] Omame A, Abbas M, Onyenegecha CP. Backward bifurcation and optimal control in a co-infection model for SARS-CoV-2 and ZIKV. Results Phys 2022;37:105481.
[17] Omame A, Okuonghae D. A co-infection model for oncogenic human papillomavirus and tuberculosis with optimal control and cost-effectiveness analysis. Optim Control Appl Methods 2021;42(4):1081–101.
[18] Md. Harun-Or-Rashid K, Akter R, Ahmed M. Forward and backward bifurcation on COVID-19 SIR model transmission. In: International conferences of physical sciences-2022. SUST, Sylhet, Bangladesh; 2022, p. 90.
[19] Kamrujjaman M, Saha P, Islam MS, Ghosh U. Dynamics of SEIR model: A case study of COVID-19 in Italy. Results Control Optim 2022;7:100119.
[20] Alshammari FS, Khan MA. Dynamic behaviors of a modified SIR model with nonlinear incidence and recovery rates. Alex Eng J 2021;60(3):2997–3005.
[21] Omame A, Okuonghae D, Nwafor U, Odionyenma B. A co-infection model for HPV and syphilis with optimal control and cost-effectiveness analysis. Int J Biomath 2021;14(07):2150050.
[22] Omame A, Isah ME, Abbas M. An optimal control model for COVID-19, zika, dengue, and chikungunya co-dynamics with reinfection. Optim Control Appl Methods 2022.
[23] Ruiz JA, De Carvalho JM. SIR model with vital dynamics for homogeneous behavior populations. 2020.
[24] Rihan F. Qualitative analysis of delayed SIR epidemic model with a saturated incidence rate. Int J Differ Equ Appl 2012;2012:13.
[25] Zakary O, Rachik M, Elmouki I. On the impact of awareness programs in HIV/AIDS prevention: an SIR model with optimal control. Int J Comput Appl 2016;133.
[26] Martcheva M. An introduction to mathematical epidemiology. Vol. 61, Springer; 2015.
[27] Ma J. Estimating epidemic exponential growth rate and basic reproduction number. Infect Dis Model 2020;5:129–41.
[28] Diekmann O, Heesterbeek J, Roberts MG. The construction of next-generation matrices for compartmental epidemic models. J R Soc Interface 2010;7(47):873–85.

[29] Paul AK, Kuddus MA. Mathematical analysis of a COVID-19 model with double dose vaccination in Bangladesh. Results Phys 2022;35:105392.
[30] Darti I, Suryanto A. Dynamics of a SIR epidemic model of childhood diseases with a saturated incidence rate: Continuous model and its nonstandard finite difference discretization. Mathematics 2020;8(9):1459.
[31] Castillo-Chavez C, Song B. Dynamical models of tuberculosis and their applications. Math Biosci Eng 2004;1(2):361.
[32] Li X, Wu R. Hopf bifurcation analysis of a new commensurate fractional-order hyperchaotic system. Nonlinear Dynam 2014;78(1):279–88.
[33] Baisad K, Moonchai S. Analysis of stability and Hopf bifurcation in a fractional Gauss-type predator–prey model with Allee effect and Holling type-III functional response. Adv Difference Equ 2018;2018(1):1–20.
[34] Wang K, Fan A, Torres A. Global properties of an improved hepatitis B virus model. Nonlinear Anal RWA 2010;11(4):3131–8.
[35] Chowell G, Ammon C, Hengartner N, Hyman J. Estimation of the reproductive number of the Spanish flu epidemic in Geneva, Switzerland. Vaccine 2006;24(44–46):6747–50.
[36] Allen LJ, Burgin AM. Comparison of deterministic and stochastic SIS and SIR models in discrete time. Math Biosci 2000;163(1):1–33.
[37] Guerrero-Flores S, Osuna O, Villavicencio-Pulido G. Different types of backward bifurcations on account of an improvement in treatment efficiency. Revista Integración 2018;36(1):21–35.
[38] Owoyemi A, Ibrahim S, Kumar P, Venkatesan G, Mamat M. Some novel mathematical analysis on the fractional-order 2019-nCoV dynamical model. Math Methods Appl Sci 2022.
[39] Owoyemi AE, Sulaiman IM, Mamat M, Olowo SE, Adebiyi OA, Zakaria ZA. Analytic numeric solution of coronavirus (COVID-19) pandemic model in fractional - order. Commun Math Biol Neurosci 2020.
[40] Owoyemi A, Ibrahim S, Mamat M, Ezekiel O. Stability and bifurcation analysis in a fractional-order epidemic model with sub-optimal immunity, nonlinear incidence and saturated recovery rate. IAENG Int J Appl Math 2021;51:515–25.
[41] Abioye AI, Peter OJ, Ogunseye HA, Oguntolu FA, Oshinubi K, Ibrahim AA, et al. Mathematical model of COVID-19 in Nigeria with optimal control. Results Phys 2021;28:104598.
[42] Sharomi O, Malik T. Optimal control in epidemiology. Ann Oper Res 2017;251(1):55–71.
[43] Hussain T, Ozair M, Ali F, ur Rehman S, Assiri TA, Mahmoud EE. Sensitivity analysis and optimal control of COVID-19 dynamics based on SEIQR model. Results Phys 2021;22:103956.
[44] Pontryagin LS. Mathematical theory of optimal processes. CRC Press; 1987.
[45] Martcheva M. Control strategies. In: An introduction to mathematical epidemiology. Springer; 2015, p. 215–48.